Extending the range measurement capabilities of modulated range imaging devices by time-frequency-multiplexing

Boris Jutzi

22. Dezember 2010

Abstract

In this contribution a time-frequency-multiplexing method for unwrapping the range ambiguity of range imaging device is presented to extend the range measurement capabilities. Beside the phase unwrapping by multiple frequency modulation a confidence measure for the range measurement is proposed. For the investigations an indoor and an outdoor scene were analyzed. The results are promising to utilize range imaging devices not only in very close range. It will be shown that four times of the manufacturers non-ambiguity range specification could be reached without modifing the sensor or improving the illumination unit.

1 Introduction

The 3D geometry of the environment is of great interest for a wide variety of applications. In order to obtain a geometric description usually the captured image or range data is analyzed, where in general a high level of automation is desirable.

By utilizing passive imaging sensors the 3D information is gained by textured image data indirectly from several images with costly stereo- or multiple image analysis. These procedures are widely used, but have indispensable claims due to capturing disposition and scene contents. For instance, the illumination conditions should be adequate, the observed materials should be textured and opaque, and the distance between object and camera as well as between the camera viewpoints of stereo images should be sufficient large for gaining a reliable 3D reconstruction.

Beside this, the photogrammetric methods are complemented by active sensor procedures. For instance, a laser scanner captures a sequence of singular range values while accomplishing a time-dependent spatial scanning of the environment. In general spaceborne, airborne as well as terrestrial laser scanner sensors allow a direct and illumination-independent measurement of 3D objects [Shan & Toth, 2008]. For an accurate data acquisition necessarily the scene contents as well as the sensor platform should be static, otherwise a deformation of the environment can appear. In general, with an increasing dynamic of the scene contents respectively sensor platform, the complexity of the analysis increases and the exploitation of 3D information is more and more challenging. To gain 3D information from rapid dynamical processes the capturing of the environment at the same time is essential.

Very recently enhanced types of active imaging sensors have started to meet these requirements, e.g. MESA with the Swiss Ranger series and PMD Vision with the CamCube series. These close ran-

ge sensors allow to capture a range image and a co-registered monochrome intensity image simultaneously with high repetition rate up to 100 releases per second. The spatial resolution can be up to 204 x 204 pixels. Beside this the non-ambiguity (sometimes called unique) range is currently about a few meters. In general the measured intensity strongly depends on the used wavelength (usually close infrared) of the laser source and the surface characteristic.

With these new types of sensors for the first time the basic principle to unify advantages of active sensors and the simultaneous capturing of an image for an extended area of dynamical 3D applications is given. Especially the 3D motion or deformation analysis, like autonomous navigation of robots, motion control for game consoles, trajectory tracking of pedestrians for surveying, or maker free 3D measurements of crash tests, are of interest. Beside the hardware and sensor developments [Lange, 2000], nowadays most works focus on geometric and radiometric calibration [e.g. Lichti, 2008] or tracking of objects or automatic extraction of object features.

The terminology for scannerless range imaging systems is multifarious, where the terms Time-of-Flight (TOF) depth camera, 3D range imager, Time-of-Flight Sensors, photonic mixer devices (PMD) [Schwarte *et al.*, 1997] or a combination of the mentioned terms are used. Most of the terms are much more related to the range measurement than to the as well available reflectivity measurement of the observed area. For the procedure the term range imaging with the abbreviation RIM is more and more established, particularly in Europe.

Especially the relatively large noise influence on the measurement, due to the large amount of ambient radiation in comparison to the emitted radiation, results in a range measurement which is less reliable compared to the performance of airborne laser scanner (ALS) or terrestrial laser scanner (TLS). The major drawbacks of the known RIM devices are:

- an absolute range accuracy of a few centimeters
- a range ambiguity of a few meters

It has to be mentioned that the range ambiguity is closely related to the well-known phase unwrapping problem which is extensively discussed in the radar interferometry community. It is a inverse problem which cannot be solved in general and intensive research is going on this issue until today. To resolve the ambiguity by phase reconstruction various methods are known in literature. A general overview of the existing methods is given in Ghiglia & Pritt [1998], where most of these approaches deal with 2D data sets. By utilizing the Goldstein 2D unwrapping procedure on RIM data an image-based solution was proposed by Jutzi [2009]. However, one large drawback of the methods is the sensitivity of the phase reconstruction to minor measurement errors. Additionally, the reconstruction suffers from multiple integer solutions caused by the unwrapping procedure. Usually the measured environment is unknown and therefore, multiple integer solutions are possible if the topography contains large geometrical discontinuities.

Beside this, from other sensor systems different techniques are known to solve this problem in order to obtain a range non-ambiguity, e.g. by utilizing at least two different modulation frequencies as most continuous-wave (CW) modulated laser scanner and radar systems do or by (pseudo) random modulation. In general, for high modulation frequencies the range measurement shows a high accuracy and the ambiguity range is small, whereas for low modulation frequencies it is vice versa. Therefore, it is always a trade-off to select the best frequency to gain optimal results.

In this paper a method for unwrapping the range ambiguity of range imaging devices is presented to extend the range measurement capabilities. In Section 2 the methodology is proposed by an overview for the measurement principle, the utilized phase unwrapping by multiple frequency modulation, and a confidence measure for the range measurement. Section 3 shows a brief overview of the utilized range imaging sensor with the selected indoor scene and the selected outdoor scene. The detailed experiments and results for both scenes are presented in Section 4. Finally, the derived results are evaluated and discussed, the content of the entire paper is concluded, and an outlook is given.

2 Methodology

In the following the measurement principle (Section 2.1), the phase unwrapping by multiple frequency modulation (Section 2.2), and a confidence measure for the range measurement (Section 2.3) are specified.

2.1 Measurement principle

The range measurement can be briefly described as follows: A sinusoidal CW modulated signal is transmitted by a LED array in form of monochromatic light (Figure 1a). The emitted light travels to the object, is backscattered by the surface and captured by a receiver unit. The receiver unit is usually a CCD or CMOS array. Single pixels of the array can be subdivided into four collaborating subpixels (Figure 1b).

Concerning a demodulation of the sinusoidal received signal the parameters amplitude A and phase shift $\triangle\varphi$ can be determined. For each measurement per single pixel four neighborhood subpixels

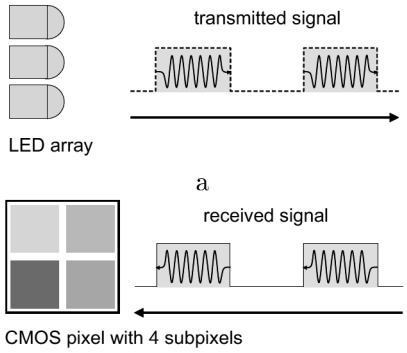

Fig. 1: Function principle of the RIM. a) transmitter, b) receiver.

are utilized to measure by time gating four intensities with a relative phase shift of 90°, or with other words an absolute phase shift of 0°, 90°, 180°, and 270° (Figure 2a). For each absolute phase shift the corresponding intensity is determined by integration. Then the phase shift $\triangle\varphi$ between the transmitted and received signal can be determined by the intensity values A_0, A_{90}, A_{180}, and A_{270} (Figure 2b) with

$$\triangle\varphi = \arctan\left(\frac{A_{270} - A_{90}}{A_0 - A_{180}}\right). \tag{1}$$

Based on the phase shift$\triangle\varphi$, the range $\triangle R$ to the object is given with respect to the two-way time of flight by

$$\triangle R = \frac{c}{2f_m}\frac{\triangle\varphi}{2\pi}, \tag{2}$$

where f_m is the modulation frequency and c the speed of light.

Unfortunately, the phase shift $\triangle\varphi$ is a wrapped phase and its corresponding range $\triangle R$ is ambiguous due to the measurement principle with the utilized modulation frequency. Hence the absolute range R to the object can not be determined directly if the real range is above the modulation range

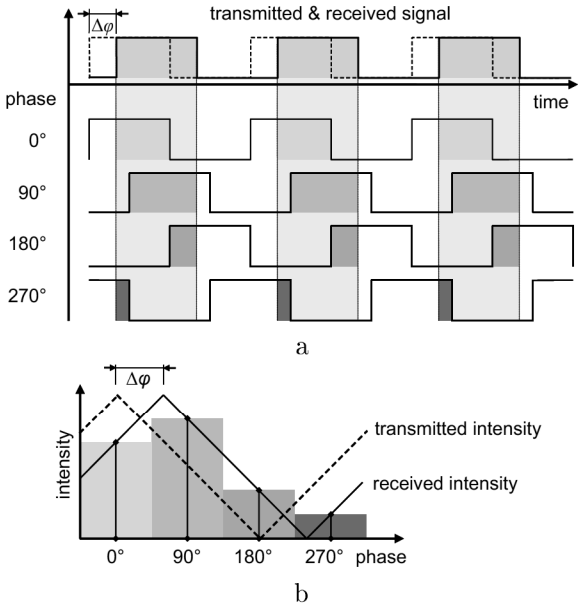

Fig. 2: Measurement principle of the RIM sensor. a) utilizing time gating to measure the phase shift, b) determining intensity by integration.

$$R_m = \frac{c}{2f_m}. \tag{3}$$

Therefore, the unwrapped phase

$$\varphi = 2\pi k + \triangle\varphi \tag{4}$$

has to be known, where the number of periods $k = 0, 1, 2, ...$ are integer valued. Based on this relationship the absolute range R can be denoted by

$$R = R_m k + \triangle R, \tag{5}$$

with the number of periods k multiplied by the modulation range R_m and added by the measured range $\triangle R$.

2.2 Phase unwrapping by multiple frequency modulation

To resolve the ambiguity of the phase measurement two different modulation frequencies f_{m1} and f_{m2} with $f_{m1} < f_{m2}$ have to be available, which results in two modulation ranges R_{m1} and R_{m2}. Additionally, two conditions have to be satisfied with $k_1 = k_2$ or $k_1 + 1 = k_2$.

Then the range measurement can be extended to a maximum range

$$R_{max} = R_{m1}k_{1max} = R_{m2}k_{2max}, \tag{6}$$

with $k_{1max} = f_1/(f_2 - f_1)$ and $k_{2max} = f_2/(f_2 - f_1)$.

Due to the two conditions two cases A and B have to be considered:

Case A

If the measured ranges are $\triangle R_1 \leq \triangle R_2$ then $k_1 = k_2 = k$ and the absolute range is

$$R = R_{m1}k + \triangle R_1 = R_{m2}k + \triangle R_2, \tag{7}$$

with $k = (\triangle R_2 - \triangle R_1)/(R_{m1} - R_{m2})$.

Case B

If the measured ranges are $\triangle R_1 > \triangle R_2$ then $k_1 + 1 = k_2 = k$ and the absolute range is

$$R = R_{m1}(k-1) + \triangle R_1 = R_{m2}k + \triangle R_2, \tag{8}$$

with $k = (\triangle R_2 - \triangle R_1 + R_{m1})/(R_{m1} - R_{m2})$.

In general, for both cases the solution for k should be integer valued.

2.3 Confidence measure for the range measurement

Due to measurement inaccuracies small variations can be expected for the calculated number of periods k_q and therefore, non-integer values will be obtained. If the non-integer value is close to the integer value it can be assumed that the calculated k_q

is reliable, if the variation is large the result is not reliable. This is of interest because due to the measurement principle in general for each pixel a range value is captured even if no surface was available. Usually the corresponding active intensity value to this range measurement should be small valued.

In order to avoid unreliable measurements it is obvious to introduce a confidence measure q for the calculated absolute range R. The confidence measure q within the intervall $[0, 1]$ can be defined by

$$q = 1 - 2 \mid k_q - \text{nint}(k_q) \mid, \tag{9}$$

with $\mid \cdot \mid$ for the absolute value and $\text{nint}(\cdot)$ for the nearest integer.

3 Configuration

A RIM sensor (Section 3.1) was utilized to capture an indoor and an outdoor scene (Section 3.2).

3.1 RIM sensor

For the investigations, a PMD Vision CamCube 2.0 sensor was used. The sensor has a 204 x 204 pixel array with a pixel size and pitch (spacing) of about 45 µm. The user can preselect the modulation frequency f_m with 18, 19, 20, and 21 MHz, which results in a modulation range R_m of 8.33, 7.89, 7.5, and 7.14 m. The maximum frame rate is about 25 frames per second and the sensor measures per pixel three features: range, active intensity and passive intensity. Therefore, above three million measurement values per second can be captured.

An example is depicted in Figure 3. For the preselected modulation frequencies $f_1 = 18$ MHz and $f_2 = 21$ MHz the range ambiguity is given by the modulation range $R_{m1}(f_1) = 8.33$m and $R_{m2}(f_2) = 7.14$m. With Formula 6 the maximum range $R_{max} = 50$ m. Furthermore, the depicted difference between $\triangle R_2$ and $\triangle R_1$ helps to understand the two different cases of interest A and B with $\triangle R_1 \leq \triangle R_2$ as positive values and $\triangle R_1 > \triangle R_2$ as negative values. At the moment, to utilize two different modulation frequencies a temporal sequential capturing of frames by alternating modulation frequencies is realized by time-frequency-multiplexing.

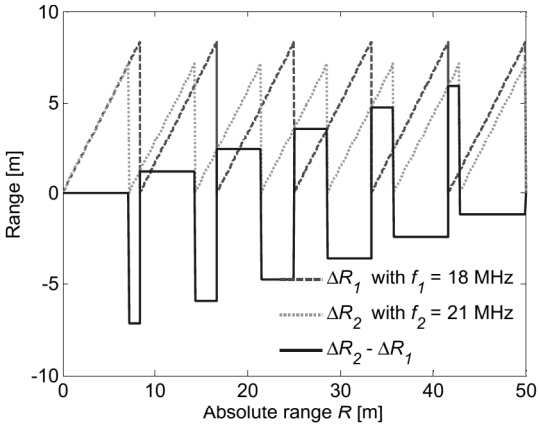

Fig. 3: Absolute range R to the object compared with measured ranges $\triangle R$ for different frequencies (dashed red and dotted green line) and calculated range differences (solid blue line).

3.2 Scene

A RIM data set of a static indoor and an outdoor scene was recorded by a stationary placed sensor. The photo of the observed scenes are depicted in Figure 4. For the environment no reference data concerning the radiometry or geometry was available.

a b

Fig. 4: Scenes captured with the RIM sensor. a) indoor, b) outdoor.

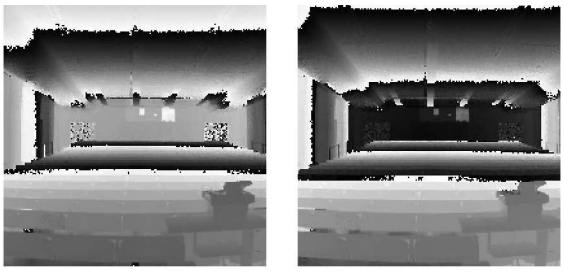

a b

Fig. 5: Range images captured with different modulation frequencies. a) $f_1 = 18$ MHz, b) $f_2 = 21.$ MHz.

4 Experiments

For the indoor and outdoor experiments the modulation frequencies $f_1 = 18$ MHz and $f_2 = 21$ MHz for maximum frequency discrimination were selected. The integration time was pushed to the maximum of 40 ms to gain a high signal-to-noise ratio for the measurement. In this case, saturation could appear in close range or at object surfaces with high reflectivity. All measurement values were captured in raw mode. Only a single image without averaging is depicted in the following figures.

4.1 Indoor

The active range measurement of the indoor scene is only sligthly influenced by additional sunlight illumination from outside and artificial lighting from the facility ceiling and therefore, a high signal-to-noise ratio is given. The two range images captured with different modulation frequencies $f_1 - 18$ MHz and $f_2 = 21$ MHz are depicted in Figure 5. Obviously the depth for modulation range R_{m1} is larger than for R_{m2} and range measurement inaccuracies can be observed, especially at the wrapping discontinuities.

Concerning the formulars in Section 2.2 the numbers of periods k_1 and k_2 can be estimated. The results for the number of periods k_2 are shown in Figure 6, where the estimated number of periods k are encoded by gray values. For the close-by ceiling and benches the estimated parameter k is close to zero. It can be observed that for larger number of periods the variations of the estimated parameter k only slightly increase. Large inconsistencies are visible at the dark colored and polished doors on the left and right side in the back of the room. Unreliable measurement values appear at the polished surfaces in the foreground mainly on the left side where the incidence angle to the surface is steep. These outliers occur due to the low reflectivity or specular surface characteristic which can result in multipath measurements. In general a non-integer value for k is not plausible (Figure 6a), therefore it was rounded to the nearest whole number (Figure 6b). Due to the size of the room for the indoor scene the number of periods is $k_2 = [0, 3]$, which can be as well observed in Figure 6 by the four different gray values.

For the estimated number of periods in Figure 6 up to three different range images can be generated, one for the non-integer and two different ones for the integer case. For each case an example is de-

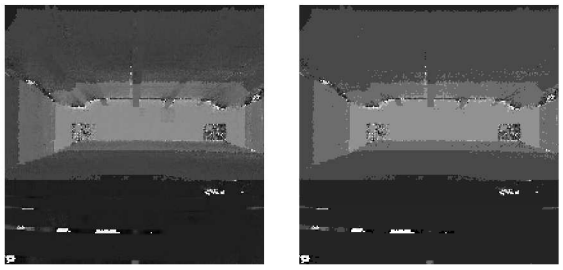

a b

Fig. 6: Estimated number of periods k_2. a) non-integer, b) integer.

picted in Figure 7. Concerning the non-integer value of the range estimation the directly calculated absolute range value is equivalent with averaging the unwrapped range values of the 18 MHz and 21 MHz measurements (Figure 7a). As one would expect, the absolute range image calculated by the integer number of periods appears cleaner with less noise. Two different absolut range images can be calculated by utilizing the 18 MHz and 21 MHz measurements. In Figure 7b the 21 MHz measurement was selected for visualization. Due to the higher modulation frequency a more accurate range measurement can be expected. However it has to be stated that it was not goal of this investigation to validate and compare these two results by a reference measurement.

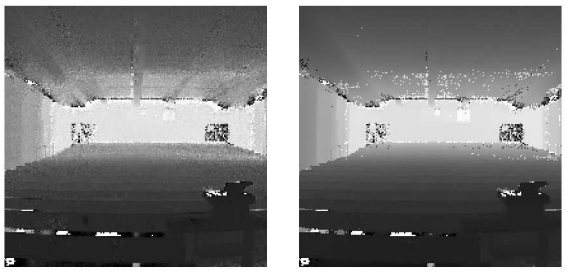

a b

Fig. 7: Unwrapped range images generated with different estimated number of periods parameters. a) non-integer number of periods, b) integer number of periods and 21 MHz measurements.

The unwrapped range values are spread over large distance, where it can be assumed that for large range values the reliability is lower due to the low signal-to-noise ratio. Figure 8a shows a histogram of the estimated absolute range values over the maximum range R_{max}, where most range values are below 23 m. Due to a maximum distance to the central wall at the back of the room of about 23 m, absolute range values above this distance are erroneous.

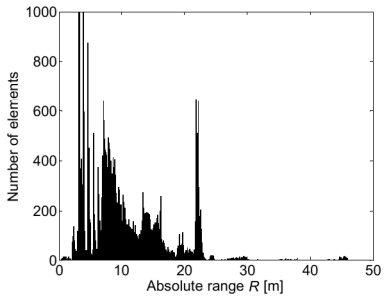

a

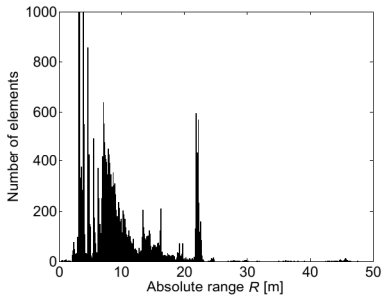

b

Fig. 8: Histogram of the absolute range values. a) all estimate values, b) for values with a confidence measure above 0.75.

To evaluate the unwrapping procedure a confidence measure q was introduced with Formula 9 and the results for the scene are visualized as image with the corresponding histogram in Figure 9. Most absolute range values over the entire scene have a high reliability except at the far away ceiling and at the polished surfaces in front, where the incidence

angle to the surface is steep. The histogram shows a widely spread distribution with a very high density close to 1, where the highest number of elements is above 0.9, but below 1. For the selected scene 77% of the absolute range values have a confidence measure above 0.75. A sample of the remaining absolute range values above this empirical preselected threshold for the confidence measure is depicted in Figure 8b.

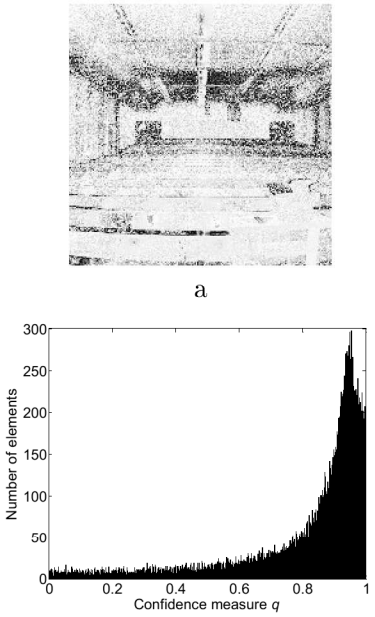

a b

Fig. 9: Confidence measure q. a) image-based visualization, b) corresponding histogram.

4.2 Outdoor

The outdoor scene provides a challenging measurement environment due to the additional influence of the background illumination by sunlight which decreases the signal-to-noise ratio of the active range measurement. The two range images captured with different modulation frequencies $f_1 = 18$ MHz and $f_2 = 21$ MHz are depicted in Figure 10, where the depth for modulation range R_{m1} is larger than for R_{m2}.

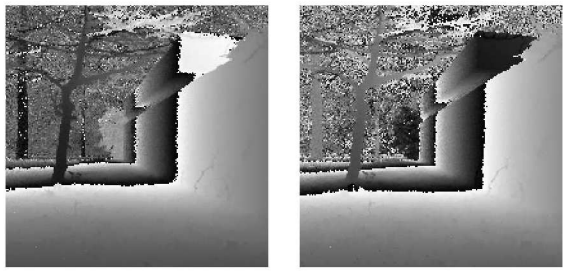

a b

Fig. 10: Range images captured with different modulation frequencies. a) $f_1 = 18$ MHz, b) $f_2 = 21$ MHz.

Again, the numbers of periods k_1 and k_2 are estimated and the results for the number of periods k_1 are shown in Figure 11. For the foreground of the image, which is obviously close-by, the estimated parameter k is close to zero. For larger number of periods the variations of the estimated parameter k increases. Again, the non-integer and integer value for k is depicted in Figure 11 for comparison purposes.

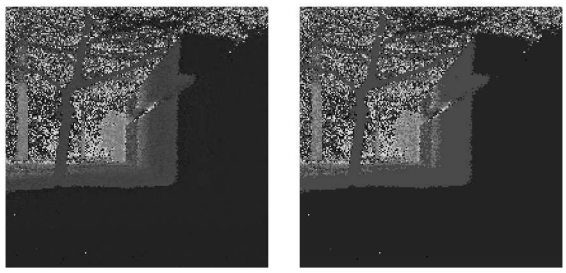

a b

Fig. 11: Estimated number of periods k_1. a) non-integer, b) integer.

For the estimated number of periods Figure 12 shows the unwrapped range images generated with

the non-integer number of periods and integer number of periods utilizing 21 MHz. Again, the range image calculated by the integer number of periods appears cleaner with less noise.

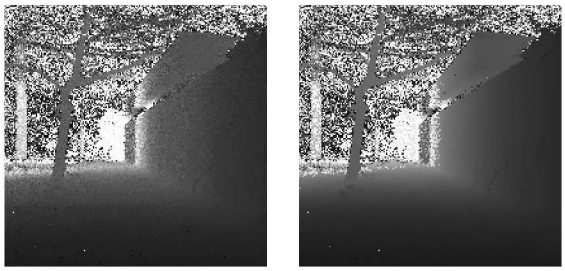

a b

Fig. 12: Unwrapped range images generated with different estimated number of periods. a) non-integer number of periods, b) integer number of periods and 21 MHz measurements.

The unwrapped range values are spread over large distance, where it can be assumed that for large range values the reliability decreases. The black bars in Figure 13a show an histogram of the estimated absolute range values, where most range values are below 15 m.

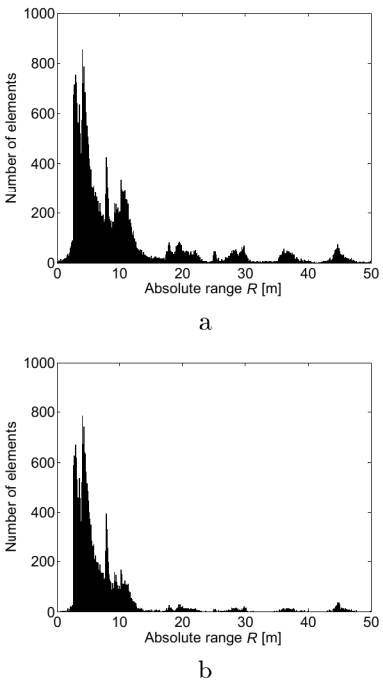

Fig. 13: Histogram of the absolute range values. a) all estimate values, b) for values with a confidence measure above 0.75.

The confidence measure q for the outdoor scene is visualized as image with the corresponding histogram in Figure 14. Again, it can be stated as it would be expected that the most reliable absolute range values appear for the close range measurements. Behind the tree, approximately at a range of 10 m, the reliabiltiy decreases. The histogram shows a widely spread distribution with a high density close to 1, where the highest number of elements is above 0.9, but below 1. For the selected scene 65% of the absolute range values have a confidence measure above 0.75. A sample of the remaining absolute range values above this empirical preselected threshold for the confidence measure is depicted in Figure 13b.

5 Conclusion

The goal of these investigations was to extend the measurement capabilities of the range. Therefore, an indoor and an outdoor scene were captured and analyzed. Even without increasing the illumination properties of the system the results are promising to utilize range imaging devices not only in very close range. Furthermore, the outdoor capability could be shown even when the results are not as good as for the indoor scene. However, the results show that four times of the manufacturers non-ambiguity range specification could be reached without modifying the sensor or improving the illumination unit, e.g.

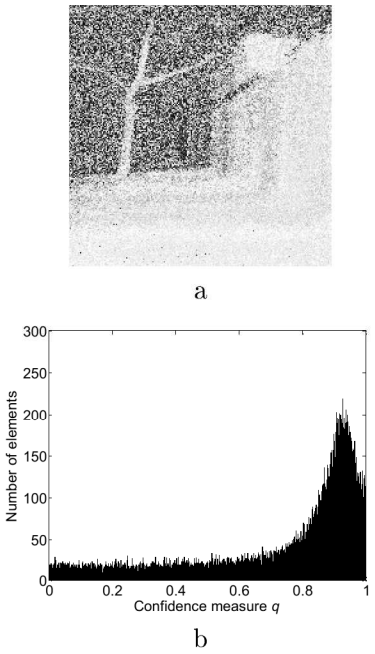

Fig. 14: Confidence measure q. a) image-based visualization, b) corresponding histogram.

by additional illumination modules.

The proposed confidence measure is a useful parameter to evaluate the range measurement and gives evidence about the measurement. It could be shown that a large number of measurements have a high confidence measure, where the highest density is only slightly below 1 (Figure 9b & 14b). On the depicted histograms it looks like a systematic error occurs which might be given by a systematic offset between the 18 MHz and 21 MHz range measurements. Therefore, further investigations have to be done which prove this assumption. However, there are different possibilities to handle this inconsistency, e.g. one is to eliminate these outliers or another is to average the two measurements derived by the different modulation frequencies. This decision can be supported by sub-dividing the confidence measure in different classes.

Usually the range imaging devices have a low range accuracy and the range measurements are sensitive to the signal-to-noise ratio. A simple possibility to increase the measurement reliability is to stretch the integration time or, with other words, to average multiple recordings, but this is of course only helpful for a static scene and a stationary placed sensor.

In future, the extended absolute range values should be validated by resolution and accuracy. Beside the restrictive static scene and a stationary placed sensor, additional investigations on more dynamic aspects should be focused. However, refined techniques might allow to gain the advantage of an extended range without loosing much data capturing speed performance.

Acknowledgement

The author would like to thank Patrick Bradley and Martin Weinmann for many valuable discussions and Christian Teutsch for assistance during the measurement campaign.

References

Ghiglia, D. C.; Pritt, M. D. (1998): Two-Dimensional Phase Unwrapping: Theory, Algorithms, and Software. John Wiley & Sons: New York. Goldstein, R. M.; Zebker, H. A.; Werner, C. L. (1988). Satellite radar interferometry: two-dimensional phase unwrapping. Radio Science, 23, pp. 713–720.

Jutzi, B. (2009): Investigations on ambiguity unwrapping of range images. In: Bretar, F.; Pierrot-Deseilligny, M.; Vosselman, G. (Eds.) Laserscanning 2009. International Archives of Photogrammetry, Remote Sensing and Spatial Information Sciences 38 (Part 3/W8), pp. 265–270.

Lange, R. (2000): 3D time-of-flight distance measurement with custom solid-state image sensors

in CMOS/CCD-technology. PhD thesis, University of Siegen.

Lichti, D. D. (2008): Self-Calibration of a 3D Range Camera. International Archives of Photogrammetry, Remote Sensing and Spatial Geoinformation Sciences 37 (Part B5), pp. 927–932.

Schwarte, R.; Xu, Z.; Heinol, H.-G.; Olk, J.; Klein, R.; Buxbaum, B.; Fischer, H.; Schulte, J. (1997): New electro-optical mixing and correlating sensor: facilities and applications of the photonic mixer device (PMD). In: Loffeld, O. (Ed.) 3D Sensors and 3D Imaging, SPIE Proceedings Vol. 3100, pp. 245-254.

Shan, J.; Toth, C. K. (Eds.) (2008): Topographic Laser Ranging and Scanning: Principles and Processing. Boca Raton, FL: Taylor & Francis.

Address of the author:

Dr.-Ing. Boris Jutzi, Institute of Photogrammetry and Remote Sensing (IPF), Karlsruhe Institute of Technology (KIT), Kaiserstr. 12, 76128 Karlsruhe, Germany, Email: boris.jutzi@kit.edu